Reconstruction of the proto-type basin and tectono-paleogeography of Tarim Block in the Mesozoic

Xiang Li[1]*, Haining Chang[1], Shaoying Huang[2], Caiming Luo[2], Yunjiang Duan[2], Hao Zhang[1], Jinkai Xia[1], Ziqi Zhong[1] and Lunyan Wei[1]

[1]The Key Laboratory of Orogenic Belts and Crustal Evolution, Ministry of Education, School of Earth and Space Sciences, Peking University, Beijing, China, [2]Institute of Petroleum Exploration and Development, Tarim Oilfield Company, Korla, China
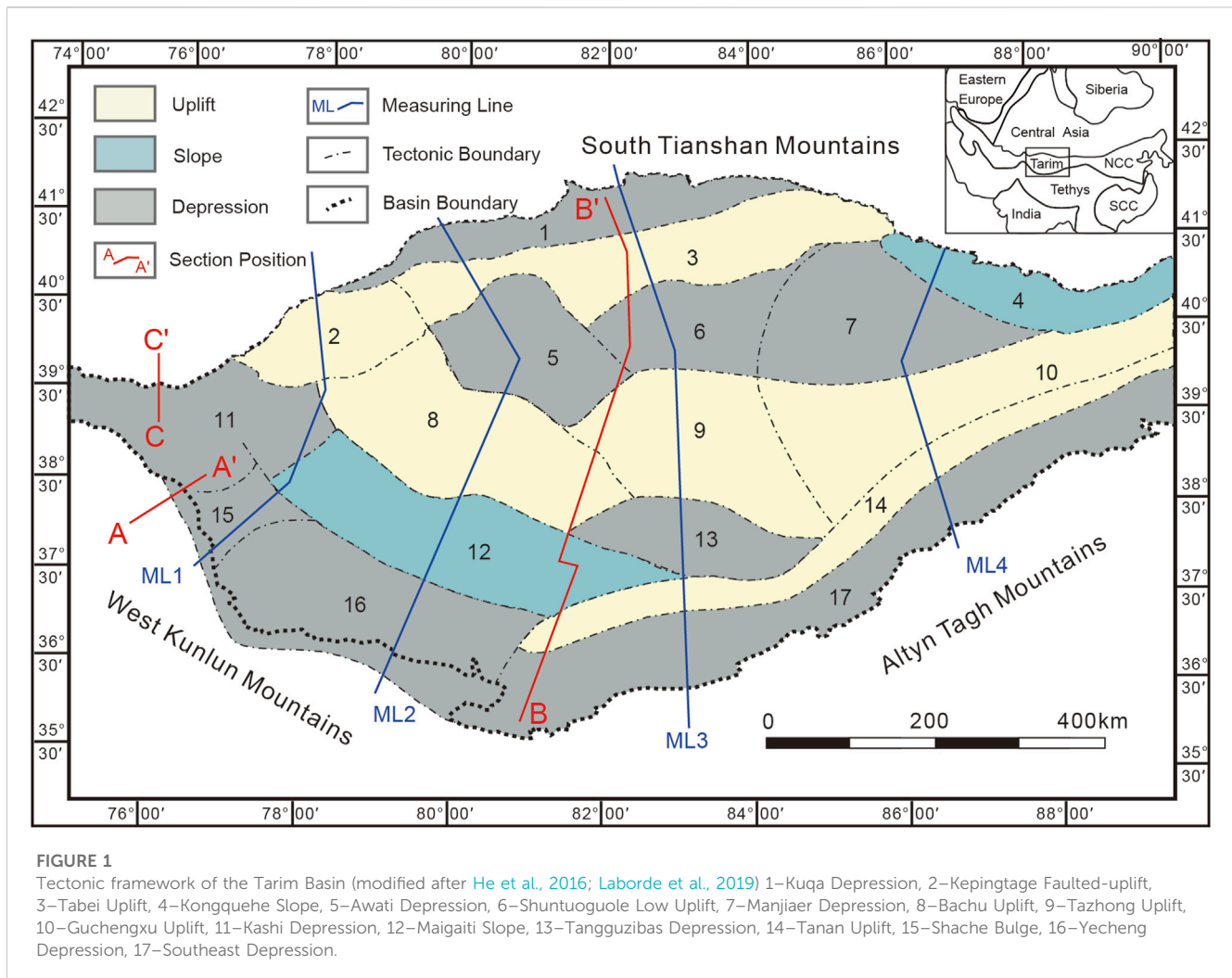
The reconstruction of the proto-type basin and tectono-paleogeography of the Tarim Basin during the Mesozoic is crucial for hydrocarbon exploration, particularly for identifying hydrocarbon source rocks. This study reconstructs the position, thickness, and distribution of the original stratigraphy, the shortening amount by structural deformation, and the distribution of sedimentary facies in each Mesozoic period using paleomagnetic data, residual stratigraphy data, seismic profiles, and lithofacies distribution. During the Triassic period, a syn-collision thrust fault structure formed in the southern Tarim Block due to the successive collision of the Tianshuihai-Bayankara terrane, North Qiangtang terrane, and South Qiangtang terrane with the Tarim Block. The sedimentary strata mainly distributed in the Northern Depression and Kuqa Depression, and their sedimentary centers continuously moved northward. In the Early-Middle Jurassic, faulted basins representing post-collision extensional structures developed on the margins of the Tarim Block. In the Late Jurassic, the Tarim Block was compressed, and the faulted basin transformed into a depressional downwarped basin with red coarse clastic sediments due to the collision of the Amdo-Dongkacuo microcontinent with the Tarim Block. In the late Early Cretaceous, the collision between the Lhasa Block and the Tarim Block caused the entire uplift of the Tarim Block, which stopped accepting deposition except for the deposition of marine facies in the southwestern Tarim Basin influenced by a large-scale transgression event. The complex evolution of the Paleo-Tethys and Neo-Tethys Oceans during the Mesozoic significantly influenced the sediment distribution and structural features of the Tarim Basin.

KEYWORDS

Tarim Basin, proto-type basin, tectono-paleogeography, Mesozoic, basin evolution

1 Introduction

The Tarim Basin, located in western China, is a large superimposed basin that underwent multiple phases of tectonic deformation from the late Neoproterozoic to Cenozoic (Figure 1; Li et al., 1996). The basin's architecture is complex and characterized by the development of a series of large-scale paleo-uplifts and tectonic non-conformities because of the drastic variation in disintegrations and collisions with the surrounding terranes in different periods. The deformation phase indicated by the extensive angular non-conformity has resulted in significant changes in the tectonic geomorphology and geography of the basin. Petroleum

FIGURE 1
Tectonic framework of the Tarim Basin (modified after He et al., 2016; Laborde et al., 2019) 1−Kuqa Depression, 2−Kepingtage Faulted-uplift, 3−Tabei Uplift, 4−Kongquehe Slope, 5−Awati Depression, 6−Shuntuoguole Low Uplift, 7−Manjiaer Depression, 8−Bachu Uplift, 9−Tazhong Uplift, 10−Guchengxu Uplift, 11−Kashi Depression, 12−Maigaiti Slope, 13−Tangguzibas Depression, 14−Tanan Uplift, 15−Shache Bulge, 16−Yecheng Depression, 17−Southeast Depression.

exploration in the basin has shown that most of the hydrocarbon accumulation was closely related to development of the proto-type and tectono-paleogeography. Thus, research on the evolution of proto-type and tectono-paleogeography of the Tarim Basin has greatly intensified over the past 2 decades (Jia and Wei, 1997; Jin and Wang, 2004; He et al., 2007; Gao et al., 2017; Wang et al., 2017; Lei et al., 2020; Wu et al., 2020; Wei et al., 2021; Xia et al., 2023; Zhong et al., 2023).

The Tarim basins we see today are the result of multiple tectonic cycles and various types of tectonic activity. Over time, the nature of these basins has changed and they have undergone different transformations. To better understand these changes, researchers use proto-type basin reconstruction which involves analyzing the current basin fill and tectonic background to uncover the original basin and analyze the effects of its transformation. Tectono-paleogeography is a field of research that examines the formation, development, and evolution of basins, and how tectonic activity affects sedimentary facies. This is achieved through the reconstruction of basins, orogenic belts, and global paleocontinents. Several studies have utilized proto-type basin and tectono-paleogeography reconstruction to gain insight into the Tarim basins (Feng et al., 2004; He et al., 2013; Chen et al., 2013;

Chen et al., 2015). Systematic analysis from the proto-type basin and tectono-paleogeography development perspective is crucial for hydrocarbon exploration due to the significant role played by reconstruction techniques in identifying the types and locations of organic rock facies belts in the basin, as well as understanding the paleo-ecological environment and sedimentary rock facies. The analysis of the tectonic setting, the proto-type and tectono-paleogeography in the Tarim Basin is of theoretical importance and exploration value to understanding of formation and development of the Tarim Basin and prediction of the favorable reservoir rock belts and play fairways (He et al., 2007; Wu et al., 2021).

The Mesozoic Tarim Basin was an intracontinental basin surrounded by orogenic belts and mostly developed terrigenous clastic deposits (He et al., 2005). The closure of the Paleo-Tethys Ocean and the opening-closing of the Neo-Tethys Ocean in the southern Tarim Basin had a powerful influence on the basin (Wang et al., 2010; Xu et al., 2011). The frequent tectonic events of the Mesozoic formed several unconformities and the denudation destroyed the original basin structure. The Mesozoic is a key time in the tectonic evolution history of the Tethysides. For the Tethysides, the oceanic crust subduction, the oceanic basins closing,

and some collision events occurred in the Paleo-Tethyan realm during the Mesozoic, and the Neo-Tethys was opened and spreading in Mesozoic (Mattern and Schneider, 2000; Xiao et al., 2015; Wu et al., 2020). The impact of Mesozoic tectonic events on the sedimentary and evolutionary history of the basin remains poorly understood due to the challenges of obtaining geological information from the basin's interior, which is covered by desert. Denudation and thrust resulting from tectonic events caused damage to the Mesozoic prototype basins, leading to ongoing debates about the nature and evolution of these basins. For example, questions remain about whether a basin containing sediments existed in the southwest Tarim Basin during the Early–Middle Triassic (He et al., 2005; Zheng et al., 2014; He et al., 2016), and whether the Triassic Kuqa depression and the Late Jurassic southwest Tarim Basin represent a downwarped basin or a foreland basin (Liu et al., 2000; Jia et al., 2003; Yang et al., 2019; Li et al., 2022).

This paper presents a comprehensive analysis of the Tarim Basin's nature and evolution, using a range of methods such as paleomagnetic, petrological, stratigraphic thickness data, and seismic profiles. Through this research, the Mesozoic proto-type basin and tectono-paleogeography of the Tarim Block have been reconstructed, shedding new light on the geological history of the region. Additionally, the study examines the impact of tectonic events on the Tarim Basin, providing insights into the factors that have shaped the basin's structure and geological characteristics over time. Overall, the findings presented in this paper contribute to a better understanding of the Tarim Basin and its complex geological history, offering valuable information for further research and exploration.

2 Database and methods

2.1 Database

For the reconstruction of the Mesozoic proto-type basin and tectono-paleogeography in the Tarim Basin, we collected the residual stratigraphic thickness data, outcrops data, wells data, and 81 seismic sections of the Tarim Basin in each period of the Mesozoic mainly from the Tarim Oilfield. The timing of the north-south collision between two terranes can be determined by the overlap of their paleolatitudes or the change of their convergence rate. For the location reconstruction, this paper mainly collected Mesozoic paleomagnetic data from various terranes around the Tarim Basin (Mcfadden et al., 1988; Li et al., 1988; Zhang et al., 1989; Li, 1990; Fang et al., 1991; Chen et al., 1992; Li et al., 1995; Fang et al., 1997; Meng et al., 1998; Fang et al., 2001; Shen et al., 2005; Gilder et al., 2003; Wang, 2004; Gilder et al., 2008; Song et al., 2012; Song et al., 2015; Ma et al., 2020; Hu et al., 2022; Wei et al., 2022).

2.2 Methods

There are three principles we need to obey when reconstructing the proto-type basin maps. Firstly, reconstruct its location, which means figuring out the paleogeographic position. Secondly, reconstruct the isopach maps of proto-type basins and the

distribution of sedimentary lithofacies. Finally, reconstruct the original range of the proto-type basin by calculating the extension or shortening amount. Detailed procedures are explained below.

1 The paleolatitude of the blocks can be obtained from paleomagnetic data compared with paleopoles, but the paleolongitude is uncertain (Hou et al., 2008). The igneous rocks representing subduction and collision and oceanic magnetic anomaly bands can determine the relationship between the terranes and whether the oceans closed or spreading. We can build a global plate distribution map based on these paleolatitudes and the relationship between the plates. In this paper we emphasize that two reliability criteria must be satisfied for inclusion in the assessment namely: 24 or more samples yielding a 95% confidence limit (A_{95}) of <16° and Q ≥ 4 (An internationally-recognized reliability index for paleomagnetic data, Van der Voo, 1990).

2 At present, the erosional thickness of major unconformities is quantitatively calculated by such means as vitrinite reflectance, paleopore analysis, and sonic well log data based on borehole information (Magara, 1976; Henry and Natalya, 1996; Liu et al, 2000). However, it is usually difficult to use only these data to map the distribution of an unconformity or its erosion amount in plane owing to limitations of the available borehole data (Lin et al., 2011). Therefore, this paper reconstructed the thickness and extent of denuded stratigraphy in different basins according to the trend surface of formation thickness, based on the residual stratigraphy information of Tarim Oilfield. In this study, we estimated the erosion thicknesses of the unconformities by analyzing the geometry of the eroded strata beneath the unconformity surfaces, as depicted in seismic profiles that have been calibrated with borehole data (Lin et al., 2012). Then, the sedimentary facies were supplemented on the extent of the original basin inferred from the existing sedimentary facies.

3 The extension or shortening amount is measured from the 81 balanced cross-sections which can eliminate the effects of structure and deformation. The amount of shortening and extension of each period can be got by comparing the length of that period with the length of the next period, combining the shortening amount from Laborde et al. (2019) since the Cenozoic. The reconstruction of the final original stratigraphic spreading is carried out according to these shortening amounts from 81 profiles averaged in eight directions (M1N, M1S, M2N, M2S, M3N, M3S, M4N, M4S). Since the deformation mainly exists at the edge of the Tarim Basin, the shortening is mainly distributed in the northern and southern margins (Table 1).

To determine the characteristics of the Kuqa Basin and the southwestern Tarim Basin, we reconstructed their distribution and deformation. Initially, we gathered information on the residual thickness and distribution of each basin in the Tarim Block. Next, we reconstructed the denuded stratigraphy of the basin perimeter using the trend surface of formation thickness method (Wu et al., 2019). To complete the reconstruction of the proto-type basin extent, we supplemented the denuded strata with sedimentary facies according to sedimentary facies distribution (Chen, 1995; Jia, 2009; Liu et al., 2012; Yu et al., 2016). Finally, to eliminate the impact

TABLE 1 The Mesozoic and Cenozoic shortening amount of the Tarim Basin (km).

Distribution of the shortening amount	Cenozoic	Cretaceous	Jurassic	Triassic
Northern margin of ML1	36	0	0	0
Southern margin of ML1	32	1.4	−0.8	2.2
Northern margin of ML2	21	0.2	−0.4	0.4
Southern margin of ML2	35	0	0	4
Northern margin of ML3	22	0.4	−0.8	0.7
Southern margin of ML3	0.9	3	−1	9.3
Northern margin of ML4	0	0	0	0
Southern margin of ML4	0.3	2	−0.7	6.1

of deformation on basin distribution, we calculated shortening or extension (Table 1) based on the balanced cross-sections (81 seismic sections) and previously published data (Chen et al., 2009; Laborde et al., 2019; Wang et al., 2020). As a result, Mesozoic proto-type basin maps were drawn based on the above reconstructions of the proto-type basin of the Tarim Basin.

3 Tarim Block in the global plate tectonics and its evolution
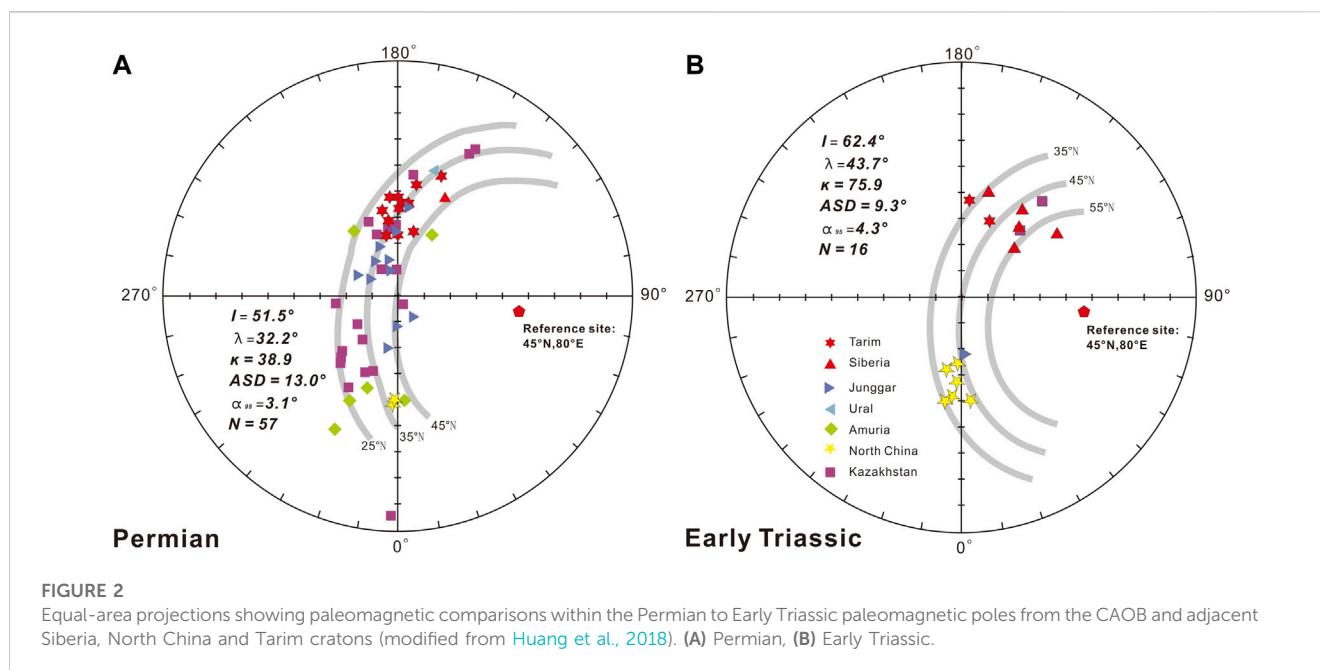
3.1 The position and orientation of Tarim Block in the Mesozoic

The Tarim Basin is a large composite and superimposed sedimentary basin developed on the crystal basement of pre-Cryogenian continental crust, whilst a large Meso–Cenozoic composite inland basin is developed on a Paleozoic platform (Zhou et al., 2001; Jia et al., 2004; He et al., 2005). The Mesozoic sediments in the Tarim Basin are mainly continental clastic rocks, primarily distributed in the Kuqa Depression, North Depression, Southwest Depression and Southeast Depression. Only the Southwest Depression developed shallow marine carbonate deposits in the late Cretaceous Tarim Basin. The main paleomagnetic data are acquired from sedimentary strata in the margins of the Kuqa and southwestern Tarim Depression due to the lack of magmatic activity in the Tarim Basin during the Mesozoic and the large area of the basin covered by the Taklamakan Desert (Li et al., 1988; McFadden et al., 1988; Zhang et al., 1989; Li, 1990; Fang et al., 1991; Chen et al., 1992; Li et al., 1995; Fang et al., 1997; Meng et al., 1998; Fang et al., 2001; Gilder et al., 2003; Wang, 2004; Shen et al., 2005; Gilder et al., 2008). The only exception has been reported from a Middle Jurassic alkali gabbro and basalt in the Tuoyun Basin of southwestern Tarim (Li et al., 1995; Meng et al., 1998; Wang, 2004; Gilder et al., 2008). The characteristic remanent magnetization here has dual polarity and consistent tilt-corrected inclinations between the gabbro and sandstone specimens of the Triassic and Jurassic seem to rule out significant inclination shallowing in the sediments. The relative rotation of the individual mean C3–T1 and J3–E1 poles has been Gilder reported between Tarim and Eurasia, which is 9.4° + 6.4° clockwise (Gilder et al., 2003). The paleomagnetic poles from Early Cretaceous redbeds in the Kuqa and southwestern

Tarim show a ~10°–15° inclination shallowing compared with coeval observations from volcanic rocks from the Tuoyun Basin in southwestern Tarim. No sizeable extensional structure is found in the north margin of Tarim Basin, and there is block limitation in the south margin of Tarim Basin. Therefore, it is the inclination shallowing of the redbeds, not the result of the massive southward movement of the Tarim Block. The pole remained at intermediate to present high latitudes throughout the Permian to the Mesozoic interval with Permian to Jurassic paleopoles identifying little or no apparent polar wander (APW) (Huang et al., 2018). Paleomagnetic data and apparent pole-shift curves show that the Tarim Block was between ~35° and 45° N during the whole Mesozoic with quasi-stationary position and direction (Gilder et al., 2008).

3.2 Relationship between the Tarim Block and the surrounding massif in the pre-Mesozoic

Numerous lines of evidence from paleomagnetic, petrological, geochronological, and paleontological studies indicate that the North Qiangtang terrane (NQT), South Qiangtang terrane (SQT), Lhasa terrane (LT), India plate, and Indochina block underwent convergence, and the Tethys Ocean gradually closed during the Permian period. Zhao et al. (2018) synthesized the most recent data and geologic evidence that place critical constraints on the closure history of the oceanic domains (Liu et al., 2015; Liu et al., 2016; Liu et al., 2017; Eizenhöfer and Zhao, 2018; Han and Zhao, 2018; Liu et al., 2018), proposed the shear closure of the paleo-Asian Ocean from west to east at 310–245 Ma, leading to the collision of Tarim Block with the Kazakhstan-Yili Central Tianshan Block at 310–285 Ma, Alex block (plus Central Qilian and Qaidam) with the Mongolia Terrane and Siberia plate at 280–265 Ma, and North China block with the Mongolia Terrane and Siberia plate at 260–245 Ma (Zhao et al., 2018). Comparison of the equal-area plot diagrams for paleopoles from the East Asia blocks/terranes in the Permian to Early Triassic interval shows most blocks/terranes in the Central Asian Orogenic Belt (CAOB) and surrounding blocks are concentrated within a narrow palaeolatitudinal band around ~35°N (Figure 2) implying that closure of the Paleo-Asian Ocean (PAO) and amalgamation of the CAOB were completed prior to the Early Triassic and that the majority of the CAOB was a quasi-rigid

FIGURE 2
Equal-area projections showing paleomagnetic comparisons within the Permian to Early Triassic paleomagnetic poles from the CAOB and adjacent Siberia, North China and Tarim cratons (modified from Huang et al., 2018). **(A)** Permian, **(B)** Early Triassic.

assemblage from the end of the Permian (Huang et al., 2018). The fragmentary tetrapod bones collected from the Lower Triassic Ehuobulak Group of Kuqa Depression indicate that the Tarim Block collaged with Eurasia at least in the Early Triassic. Terrestrial tetrapod fossils from the East Asian blocks (North China, South China, Tarim, Alex-Hexi-Qilian, Indochina) suggest that these blocks were already connected in the Early Triassic, allowing non-marine tetrapods to migrate between the blocks (Liu et al., 2020). These suggest that massifs (Kazakhstan-Yili Central Tianshan, Junggar, Alex, Qaidam, South China, North China, Mongolia Terrane and other East Asian blocks) in the northern and eastern Tarim collaged as part of the Eurasian continent and that the ancient Asian Ocean was closed in Central Asia before the early Triassic.

3.3 Relationship between the Tarim Block and the surrounding massif in the Mesozoic

The formation and rapid northward movement of the Cimmerian continent in the south of the Tarim Block in the early Permian to Late Triassic involved the opening and closing of Tethyan oceans and the rifting, drifting and collision of multiple continental blocks. Two significant paleomagnetic poles from sandstones of the SQT and the NQT show paleolatitudes of 27°N and 27.8°N, respectively, and indicate that the NQT was already collaged with the Tarim Block at ~220 Ma (Song et al., 2012). Song et al. (2015) reported the first volcanic-based paleomagnetic results from Triassic rocks of the Qiangtang block that appeared to average secular variation well enough to yield a reliable paleolatitude estimate. Combined with the published paleomagnetic data of the Qiangtang block, the latitude of the NQT in the Late Triassic was calculated to be 31.7 ± 3.0°N (Song et al., 2015). The first Paleozoic paleomagnetic data from the basalt of SQT indicate that it was located at a latitude of 22.3 ± 5.8°S during the middle Permian and drifted rapidly

northward with the Cimmerian blocks in early Permian to Late Triassic time. According to a simple interpolation between the paleolatitude determined from the paleomagnetic of the NQT and its surrounding blocks/terranes the early Permian to Late Triassic, the NQT collaged with Laurasia and SQT in the late Triassic (Figure 3; Wei et al., 2022).

Based on comparing these paleomagnetic evidence, this paper proposed that the NQT drifted ~50° northward rapidly during the Permian and Triassic and was collocated with Laurasia but not yet with SQT (4° difference) at ~220 Ma. The pillow basalt (~223 Ma) erupted underwater, the gabbro (~220 Ma) composed of normal mid-ocean ridge (N-MORB) fraction, the Nadi Kangri basalt (~220 Ma) formed in a continental rift setting and the peraluminous S-type granite (~222 Ma) associated with the subduction collision indicate that the Paleo-Tethys Ocean was still subducting and colliding with SQT which not yet collaged with Laurasia (Li et al., 2006; Wang et al., 2007; Fu et al., 2010; Zhang et al., 2014; Li et al., 2015). The muscovite peraluminous granite (~214 Ma) formed through magmatic underplating delamination represents SQT and NQT have been collaged at 214 Ma (Li et al., 2015). As a result of the above paleomagnetic, geochronologic, and petrological evidence, this paper proposes that the SQT and NQT terranes successively collided in Laurasia rather than merging into the NQT first and then SQT colliding in Laurasia.

Li et al. (2016) compiled existing data published mainly in Chinese literature and provided a new, high-quality, well-dated paleomagnetic pole from the ca. 180 Ma Sangri Group volcanic rocks of the LT that yields a paleolatitude of 3.7°S ± 3.4° (Li et al., 2016). This new pole confirms a trend in the data that suggest that Lhasa drifted away from Gondwana in the Late Triassic instead of Permian as widely perceived (Xu et al., 2011; Song et al., 2015; Li et al., 2016; Li et al., 2022). This drift history is constrained by geological and paleomagnetic evidence. The Lhasa terrane was located adjacent to northern Gondwana in late Triassic time, with rifting starting around 235 Ma (Zheng et al., 2018), and
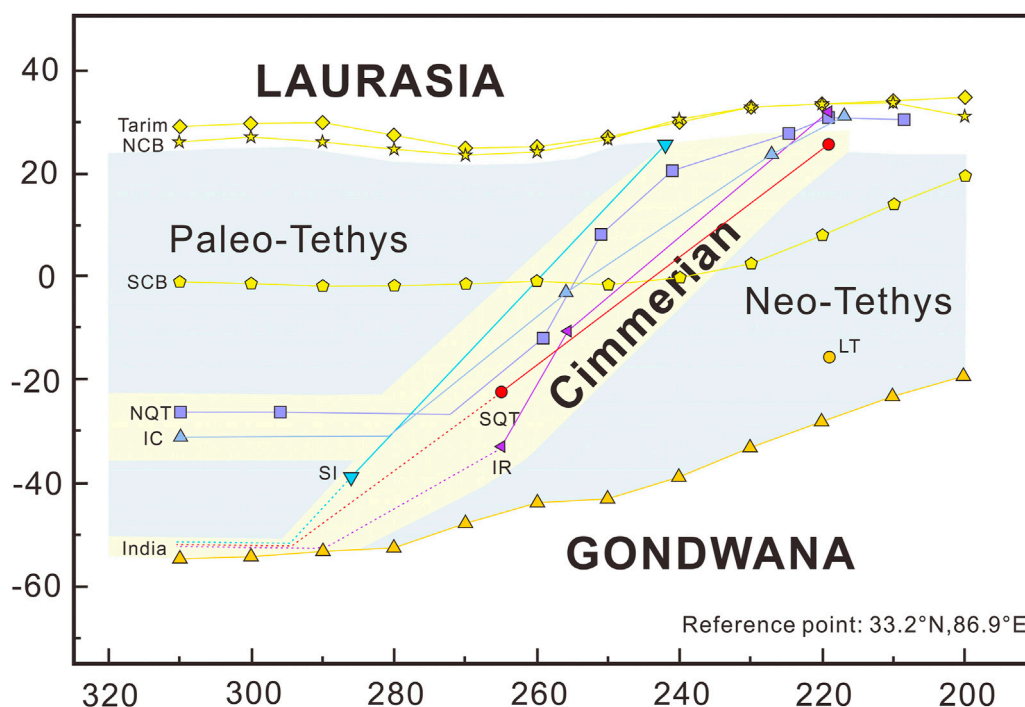
FIGURE 3
Paleolatitude evolution of the SQT and its surrounding blocks during the early Permian to Late Triassic (modified from Wei et al., 2022).
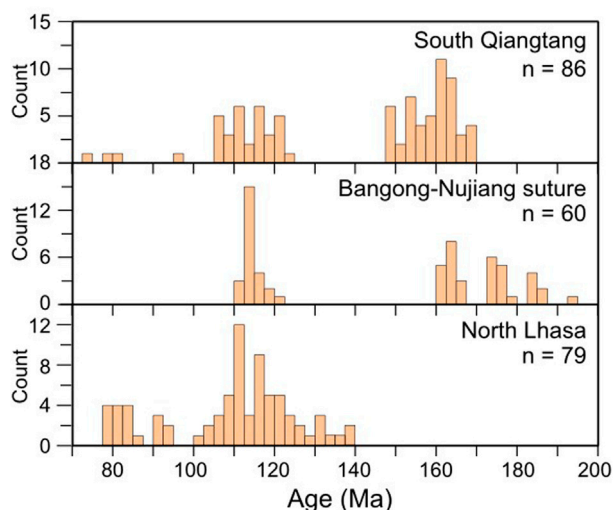

FIGURE 4
Histograms of the ages of Jurassic–Cretaceous magmatic rocks in South Qiangtang, Bangong-Nujiang suture zone, and North Lhasa (Hu et al., 2022).

northward drift occurring mostly after ~215 Ma (Li et al., 2016). The Amdo-Dongkacuo microcontinent between NQT and LT began to collide with SQT at 166–163 Ma according to the unconformity of the Dongqiao Formation with the ophiolite (Ma et al., 2020) and alluvial fan deposits sourced from the Amdo basement (Li et al., 2019), resulting in the closure of the Dongqiao-Amdo oceanic

seaway. Paleomagnetic data from the western segment of the LT indicate a paleolatitude of $20.6 \pm 5.0°N$ at ~132–106 Ma suggesting that the LT had already collided with Eurasia by this time (Chen et al., 2012). The large number of igneous rocks showing subduction, collision, and crustal thickening is concentrated in two ages, ~110–130 Ma and ~150–170 Ma, also indicating two collisions associated with Amdo-Dongkacuo (AD) microcontinent and LT (Figure 4; Hu et al., 2022).

This paper concludes that the position of the Tarim Basin remained unchanged during the Mesozoic except for a slight rotation and that the NQT, SQT, AD, LT collided successively on the southern margin of the Tarim, based on the above paleomagnetic, petrological, geochronological, stratigraphic, and paleontological data. Therefore, the global plates distribution map centered on Tarim in the Mesozoic (~220 Ma, ~160 Ma, ~120 Ma; Figure 5) was drawn on the basis of these insights, and the other plate locations were mainly referred to the data in Huang et al. (2018); Zhao et al. (2018).

4 Reconstruction of the proto-type basin

There are two major controversies related to the nature of each depression in the Tarim Basin during the Mesozoic. The first is whether a foreland basin existed during the Triassic in the southwestern Tarim, and the second is whether the Kuqa Basin was a depression or a rejuvenated foreland basin during the Triassic. In the southwestern Tarim, He et al. (2013) suggested that the southwestern Tarim region suffered denudation due to intense uplift influenced by the closure of the Paleo-Tethys Ocean and locally
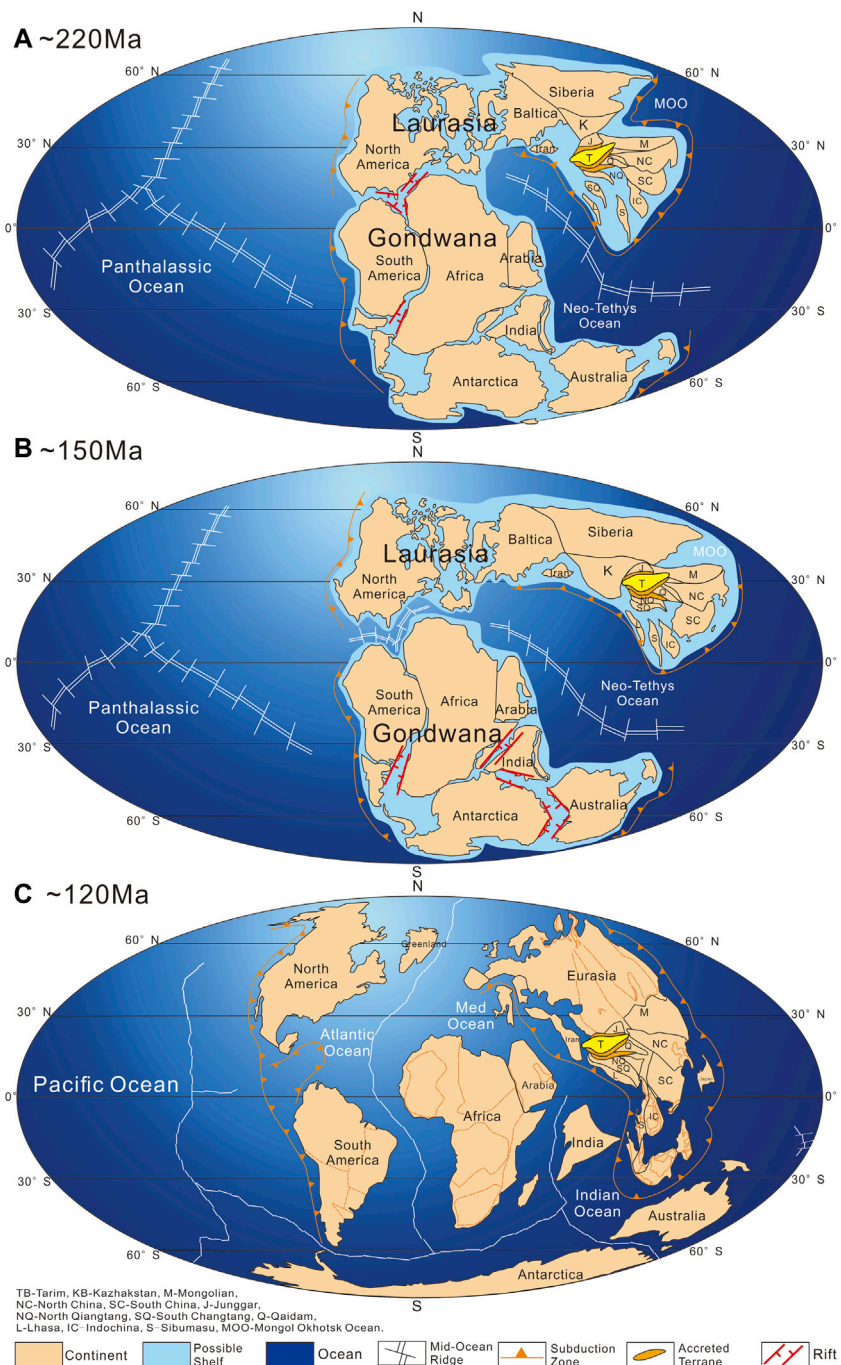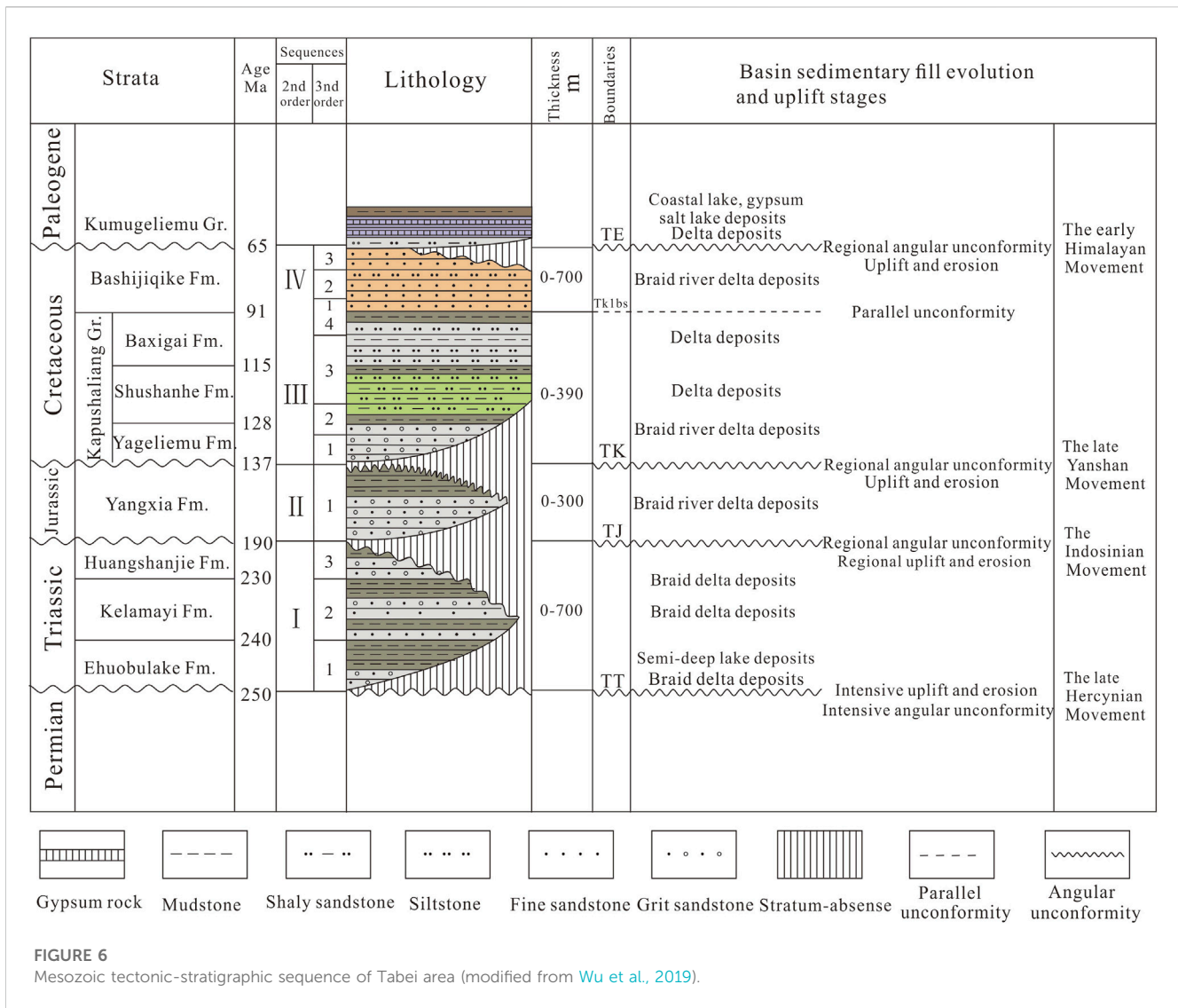
FIGURE 5
Reconstruction of global plates distribution in the Mesozoic (modified from Huang et al., 2018; Wei et al., 2022). **(A)** 220 Ma, **(B)** 150 Ma, **(C)** 120 Ma.

developed mountain basin (He et al., 2013). Zheng et al. (2014) concluded that downwarped basins should have existed in the southwestern Tarim area in the Triassic by reconstructing the proto-type basin. However, the intense uplift destroyed the sedimentary basins in the Late Triassic (Zheng et al., 2014). In the Kuqa area, Liu et al. (2000); Jia et al. (2003) considered that the Kuqa Basin belongs to the foreland basin in front of the South Tianshan folded orogenic belt in the Triassic. Qu et al., 2004; Li et al., 2017 consider the Kuqa Basin as a regional downwarped basin above

the northern margin uplift of the Late Paleozoic Tarim Block in the Triassic period.

4.1 Triassic

The Triassic stratigraphy in the Tarim Basin is mainly located in the Kuqa Basin, Tabei and Tazhong areas, and is dominated by alluvial fan-braided river delta-flood plain-lake

FIGURE 6
Mesozoic tectonic-stratigraphic sequence of Tabei area (modified from Wu et al., 2019).

facies (Figure 6; Jia et al., 2013; Wei et al., 2021). The Triassic stratigraphy (0–300 m thickness) is widely distributed in an east-west strip throughout the Kuqa Basin. The depocenter of the basin formed by the combined area of Tabei and Tazhong is in the Awati depression. Based on thickness trends, the stratigraphic thickness of the Triassic denudation may locally reach 500 m, with the original boundary line typically 2–4 km and up to 10 km from the current stratigraphic boundary line of the remnant. The width of the denuded Triassic area is 30–40 km in the northern Kuqa Basin, and the denuded thickness is 0–2,400 m (Yu et al., 2016). The balanced cross-sections can be seen that the main Triassic deformation occurred in the southwestern Tarim Basin (~3 km) and the southeastern Tarim (~7 km).

In the southwestern Tarim Basin, few Triassic strata are remained, only the Duwa site (Figure 9A) developed the Lower Triassic Wuzunsayi Formation of 200–300 m thick river-lake facies sandstone and dark mudstone in the Triassic. The Wuzunsayi Formation is conformably overlying the Upper Permian Duwa Formation with synchronous deformation and

unconformably overlain by the Jurassic-Cretaceous strata conformity, which was parallel unconformity (Yang, 1994). The Late Triassic thrust structures were also revealed by seismic interpretation (Li et al., 2017). On the seismic sections, the Late Triassic thrusts cut through the Paleozoic and stop at the bottom of the Jurassic–Cretaceous (Figure 7), and the deformations in the Jurassic–Cretaceous are similar to the overlying the Cenozoic both not involved in the Late Triassic thrusting. These may be critical evidence for developing a small basin at the Duwa of the southwestern Tarim Basin in the Early Triassic but were destroyed by thrust faults in the Late Triassic.

In the Kuqa Basin, both the remnant stratigraphy and the reconstructed primary stratigraphy show that the depocenter moved toward the orogenic zone and that the thickness thinned gradually from the depocenter to the orogenic zone. However, the depocenter of the foreland basin commonly moves toward the foreland and gradually thins from the orogenic belt to the basin. The Triassic strata are overlain on top of the South Tianshan orogenic wedge and show a progressive change in sedimentary facies and sequence structure with the overlying Jurassic strata.
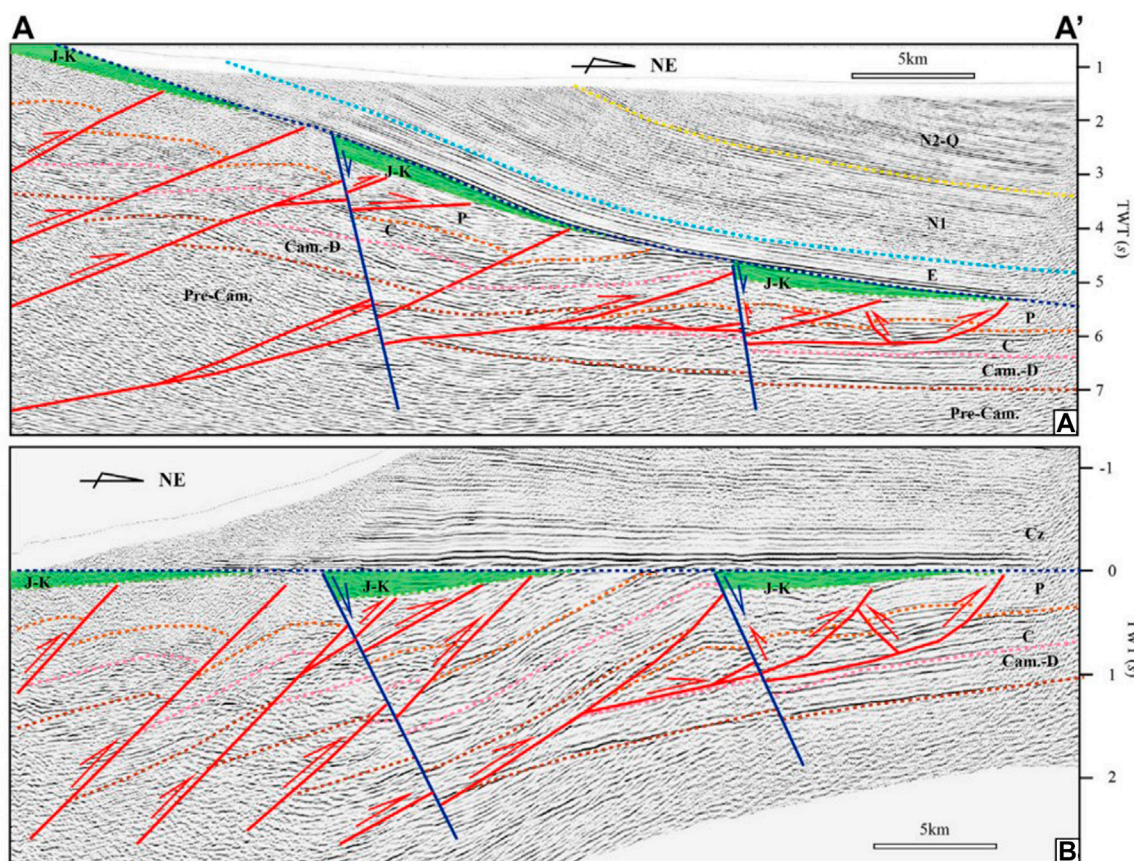
FIGURE 7
Two-dimensional seismic section A-A′ in piedmont of W. Kunlun **(A)** and flattened its Paleogene bottom **(B)** (Li et al., 2017).

As a result, the Kuqa Basin is more like a downwarped basin superimposed on the transition zone between the South Tianshan orogenic belt and the Tarim Craton. The balanced cross-sections of B-B′ (Figure 8) and Qi et al. (2022) also show that the Triassic basin did not develop large-scale thrust faults, and even normal faults may exist. Thus, the Kuqa Basin is a downwarped basin developed on top of the Late Paleozoic thrust-fold wedge or even a faulted basin in the Triassic.

The reconstruction of the Triassic proto-type basin in the Tarim Basin indicates that the Kuqa Basin and the Tazhong Basin are downwarped basins controlled by crustal isostasy (Figure 9A). There was also a local downwarped basin in the southern Tarim Basin in the Early Triassic, which was destroyed by thrust faults in the Late Triassic.

4.2 Jurassic and Cretaceous

There are three main controversial types of Jurassic faulted basins in the southwestern Tarim: the pull-apart basin associated with the Fergana-Kashgar-Yecheng strike-slip fault (Sobel, 1999), the large half-graben faulted basin between Tarim Block and West Kunlun orogenic belt (Zhang et al., 2000), and small horst-graben structure after the collision orogeny (Li et al., 2017). To address this

issue, we reconstructed the Jurassic and Cretaceous proto-type basins of the Tarim Block in the same way as above and obtained Figures 9B, C.

Jurassic formations in the Tarim Block are mainly found in the Kuqa Basin, the southwestern Tarim Basin, the southeastern Tarim Basin and the eastern Tarim Basin. The continental clastic rocks of alluvial fan-braided river delta-flood plain-lake facies are developed under the control of normal faults in the Kuqa Basin, the southwestern Tarim Basin, and the southeastern Tarim Basin. The maximum thickness of Jurassic strata in each basin is ~1,000–2000 m, and it gradually thins from the fault to the basin (Wei et al., 2022). The depocenter of the basin gradually moved toward the orogeny. Deformation in the Late Jurassic led to uplift and denudation, resulting in the formation of a regional unconformity with a general denudation thickness of 0–250 m in the interior of the basin and a maximum denudation thickness of 500 m. However, the denudation thickness is up to 2000 m, and the denudation distance is up to 40 km in the northern margin of the Kuqa basin (Yu et al., 2016). Jurassic basins are predominantly unshortened and developed faulted basins in regional extensional settings.

The Late Jurassic is a transitional phase from the stable stage of fault subsidence to the initial stage of depression. The underlying faulted basin combines with the overlying downwarped basin to form a basin with a binary structure from observation of the seismic
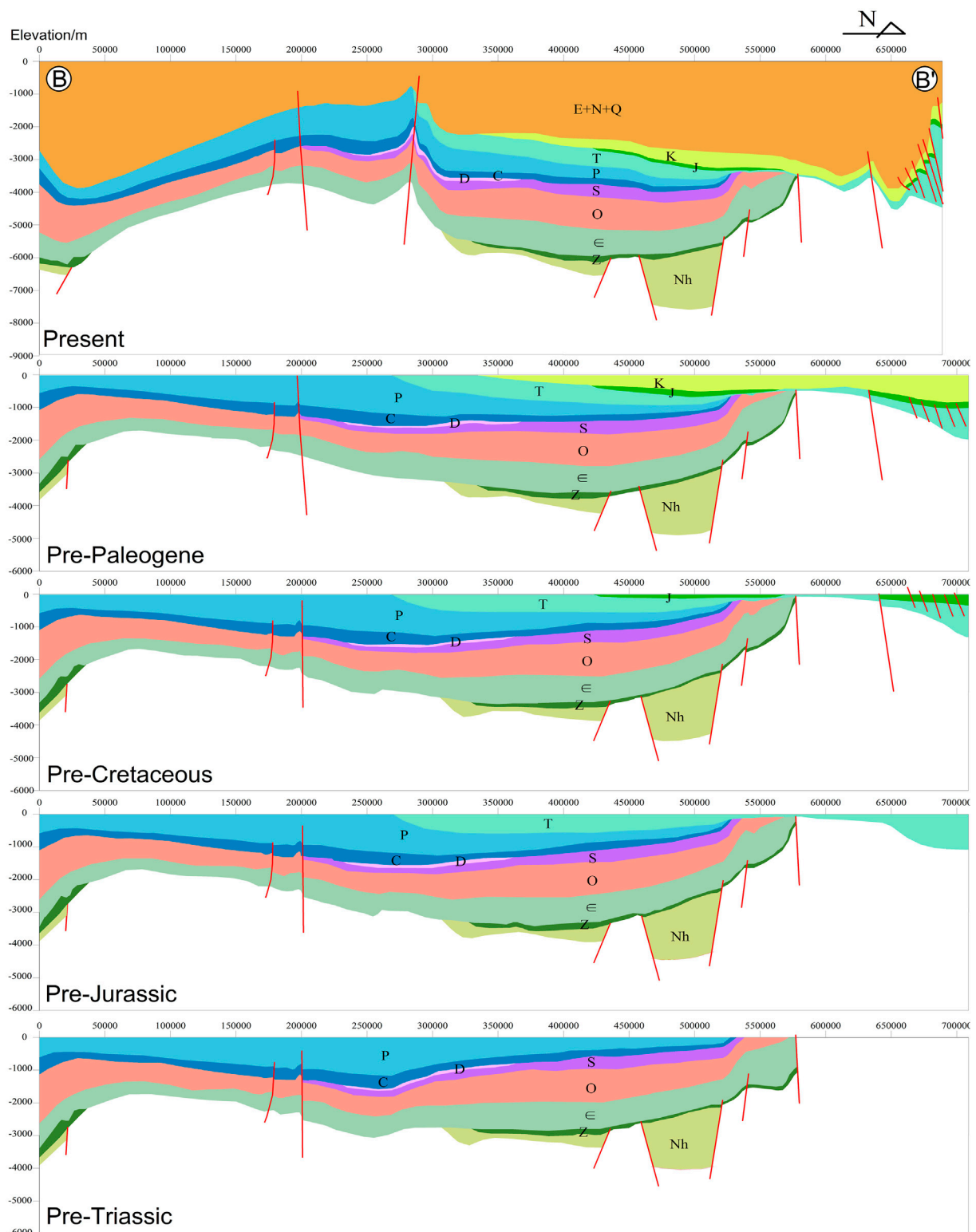
FIGURE 8
The balanced cross-section of B-B′ section. Abbreviations: Nh−Nanhua system (Cryogenian system), Z−Sinian system (Ediacaran system), ∈−Cambrian system; O−Ordovician system; S−Silurian system; D−Devonian system; C−Carboniferous system; P−Permian system; T−Triassic system; J−Jurassic system; K−Cretaceous system; E−Paleogene system; N−Neogene system; Q−Quaternary system.
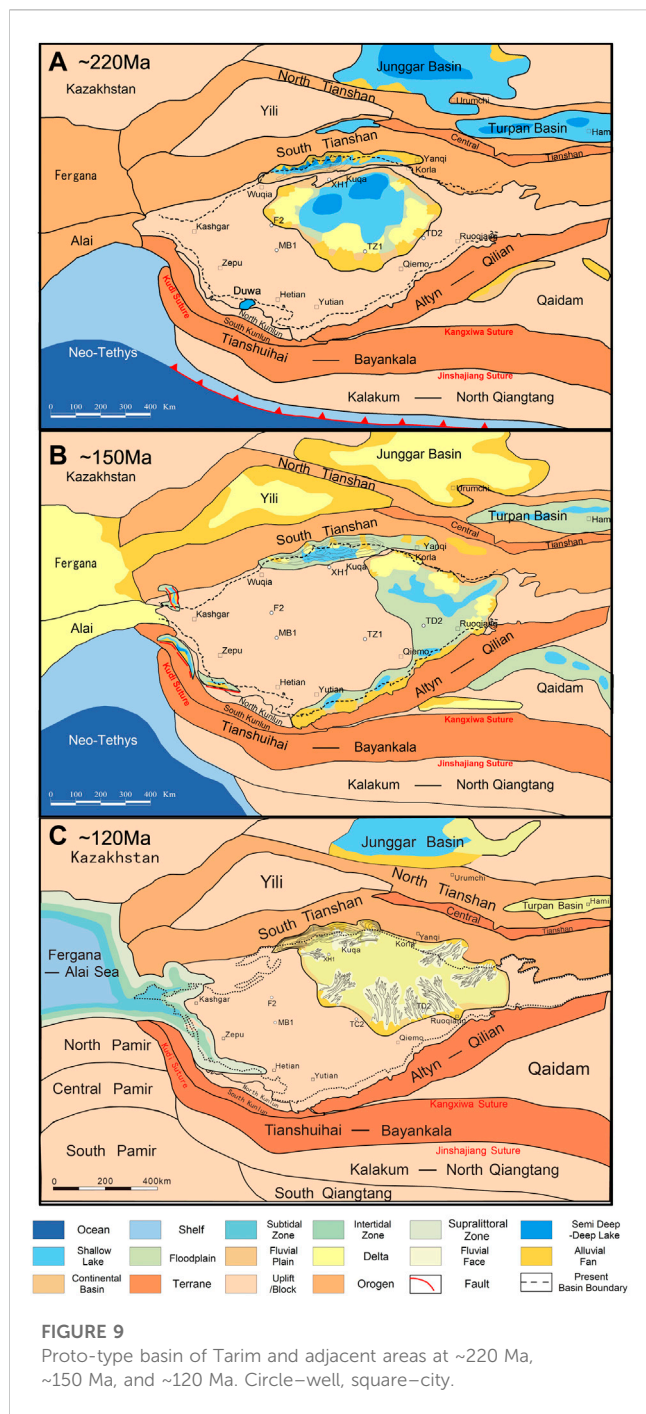
delta setting (Wu et al., 2021). These basins were not unified as one but existed in the graben-horst structure. These Jurassic basins are distributed along the Karakorum premontane faults and cannot be extended to the Ferghana Fault as no contemporaneous Jurassic clastic deposits exist between the Karakorum and the Western Tianshan. Therefore, based on reconstructions of proto-type basins, the southwest Tarim Basin was a faulted basin with small horst-graben structure after the collision of orogeny during the Jurassic.

The Early Cretaceous strata are mainly distributed in the southwestern Tarim Basin and the Central Basin consisting of Kuqa, Tazhong, Tadong, Tanan, and southeastern Tarim, and deposit red coarse clastic terrestrial deposits of alluvial fan-braided river delta-flood plain-fluvial faces. Compared to the Late Jurassic strata, the Cretaceous strata are thinner in thickness and slower in deposition rate but are similar in depositional and structural characteristics without being controlled by faults (Li et al., 2017; Wu et al., 2021). The crustal shortening did not alter significantly in most areas, except for the southeastern Tarim, where a shortening of 2–3 km occurred, resulting in a substantial uplift that reduced the area of the southeast Tarim Basin by approximately half in the Early Cretaceous. The Central Tarim Basin is an intracratonic depression basin according to these sedimentary features. During the Late Cretaceous, the Tarim Basin was denuded due to general uplift, resulting in practically no sedimentary record for the entire basin, except for the southwest Tarim Basin. The late Early Cretaceous in the northeastern part of the eastern Tethys witnessed a large-scale transgression event that resulted in the formation of the trumpet-shaped bay in the western Tarim Basin (Xi et al., 2020). Finally, the basin is dominated by repeated deposition of multiple mudstone-carbonate assemblages in the Late Cretaceous (Bosboom et al., 2014), indicating that the sedimentary environment is mainly controlled by multiple transgression-regressive cycles rather than intense tectonic activities (Zhang et al., 2018). The inconspicuous shortening of the crust and the inactive thrust faults indicate that southwest Tarim Basin was a downwarped basin throughout the Cretaceous.

The Jurassic and Cretaceous proto-type basin reconstructions (Figures 9B, C) show that the Jurassic was a fault-basin period and began a transition to a downwarped basin in the Late Jurassic. The early Cretaceous basins were deposited and sequenced in a similar manner to those of the Late Jurassic. However, unlike the Late Cretaceous Tarim Basin, which experienced uplift and ceased deposition (Jia et al., 2003; Jin et al., 2008), except for the southwest region where there was the development of marine sedimentation due to multiple transgression-regression cycles.

5 Reconstruction of tectono-paleogeography around the Tarim Basin

The study of tectono-paleogeography focuses on tectonic patterns and paleogeographic features. The basin types and global tectonic events control the paleogeographic distribution, basin subsidence rates, depositional systems and evolution of proto-type basin. The Tarim Basin has entered the stage of continental basin development since the Mesozoic and mainly developed

section in Jurassic (Figure 10). An approximately 60 km-wide Triassic fold-and-thrust belt along the southwestern margin of Tarim Basin is unconformably overlain by a Jurassic–Cretaceous sedimentary sequence along a regional angular unconformity in the southwestern Tarim Basin. The Lower–Middle Jurassic strata consists mainly of an upward-fining sequence ranging from terrestrial conglomerates to turbidite deposits, representing the products of an initial rift stage. Contrast to the pioneering phase, the sequence of Late Jurassic through Early Cretaceous were characterized by several cycles of coarse clastic deposits with large-scale cross laminations that suggest a fluvial to braided
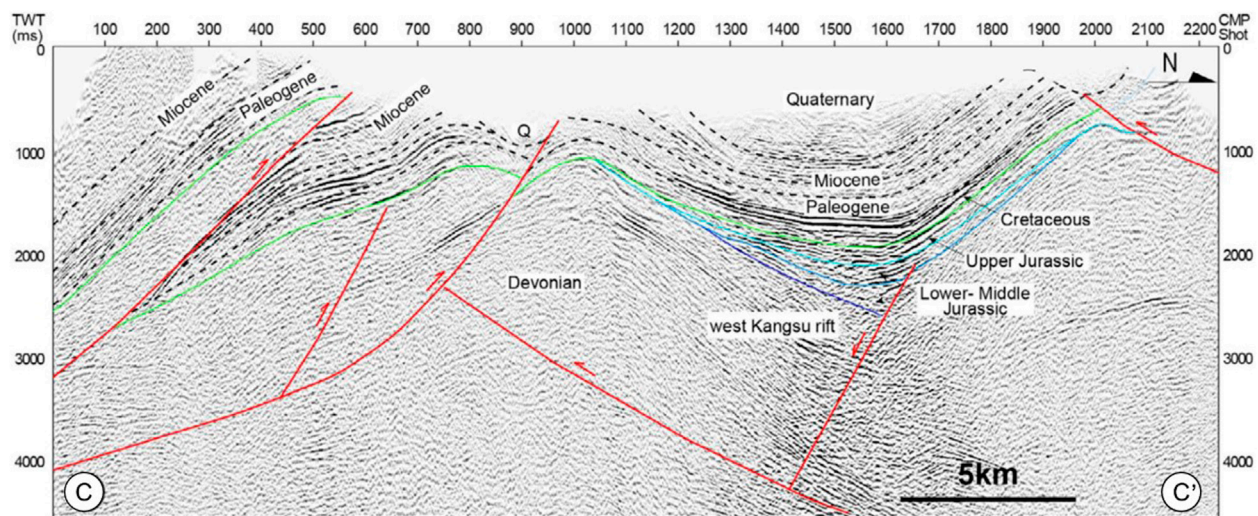
FIGURE 10
Interpretation of the seismic profile C-C′ in the southwestern Tarim Basin (Wu et al., 2021).

terrestrial clastic rocks (He et al., 2005). The closure of the Paleo-Tethys Ocean and the opening-closing of the Neo-Tethys Ocean in the southern Tarim Basin heavily influenced the Tarim Basin, including changes its uplift-depression pattern and unconformity development (Wang et al., 2010; Xu et al., 2011). In order to clarify the influence of global tectonic events on the Mesozoic paleogeography of the Tarim Basin, this paper analyses the Mesozoic geotectonic events on the periphery of the Tarim Basin and reconstructs the Mesozoic tectono-paleogeography of the Tarim Basin in a comprehensive view.

5.1 Tectono-paleogeography around the Tarim Basin in the Late Triassic period

The Paleo-Tethys Ocean had begun to northward subduction since the Carboniferous in the southern Tarim and eventually closed in the Late Triassic in response to the accretion of the Tianshuihai-Bayankara terrane, NQT and SQT with the Tarim Block (Jolivet et al., 2001; Xiao et al., 2002; Xiao et al., 2003; Liu et al., 2015; Song et al., 2015; Ma et al., 2020; Wei et al., 2022). The intense compressional collision caused an uplift in the southern Tarim Basin, transforming the Permian foreland into an uplift (He et al., 2015). This collision also formed the thrust fault structure from the West Kunlun orogenic belt and the Altyn orogenic belt toward the basin in the southern margin of the Tarim Basin, as well as the back thrust structure from the basin to the orogenic belt in the Maigaiti slope (Li et al., 2017). Uplift and thrust of the basin caused the Early–Middle Triassic strata in Bachu, Tanggu and Tadong areas to be denuded to the Central basin and formed a sizeable regional unconformity. Alluvial fan-braided river delta-flood plain-lake facies were mainly developed in the central basin, and the depocenter was located in the Tabei area and moved northward continuously during the Triassic period (Liu et al., 2012). At this time, Kuqa Basin, as a downwarped basin superimposed on the

transitional zone between the northern margin uplift of the Tarim Craton and the Late Paleozoic southern Tianshan orogenic wedge, was not evidently affected by the collision (Figure 11A).

5.2 Tectono-paleogeography around the Tarim Basin in the Late Jurassic period

The Tethys region was in an expanding setting as the New Tethys Ocean spread during the Early to Middle Jurassic. The Triassic uplift transformed into depressions in the southern Tarim Basin under the extensional background, and a series of narrow and deep faulted basins with coal-bearing strata composed of sand-mudstone intercalated with coal seams at the margin of the Tarim Basin (Figure 11B). The Amdo-Dongkacuo microcontinent collided with the southern margin of Tarim during the Late Jurassic period, which caused the Tarim Basin to be influenced by compressional stresses (Ma et al., 2020). The normal fault ceased to be active and the graben basin began to transform into a downwarped basin. Red coarse-grained clastic rocks were deposited throughout the basin during the Late Jurassic, and alluvial fans suddenly appeared in the southeastern Tarim.

5.3 Tectono-paleogeography around the Tarim Basin in the late Early Cretaceous period

The collision of the Amdo-Dongkacuo microcontinent with the Tarim Block in the Late Jurassic represents the beginning of the collision of the paleo Lasa terranes with Eurasia. The northward subduction of the Meso-Tethys during the Early Cretaceous and the continued collision of microcontinents created continuous compressional stress on the Tarim Basin. The southeastern Tarim began to uplift and no longer received
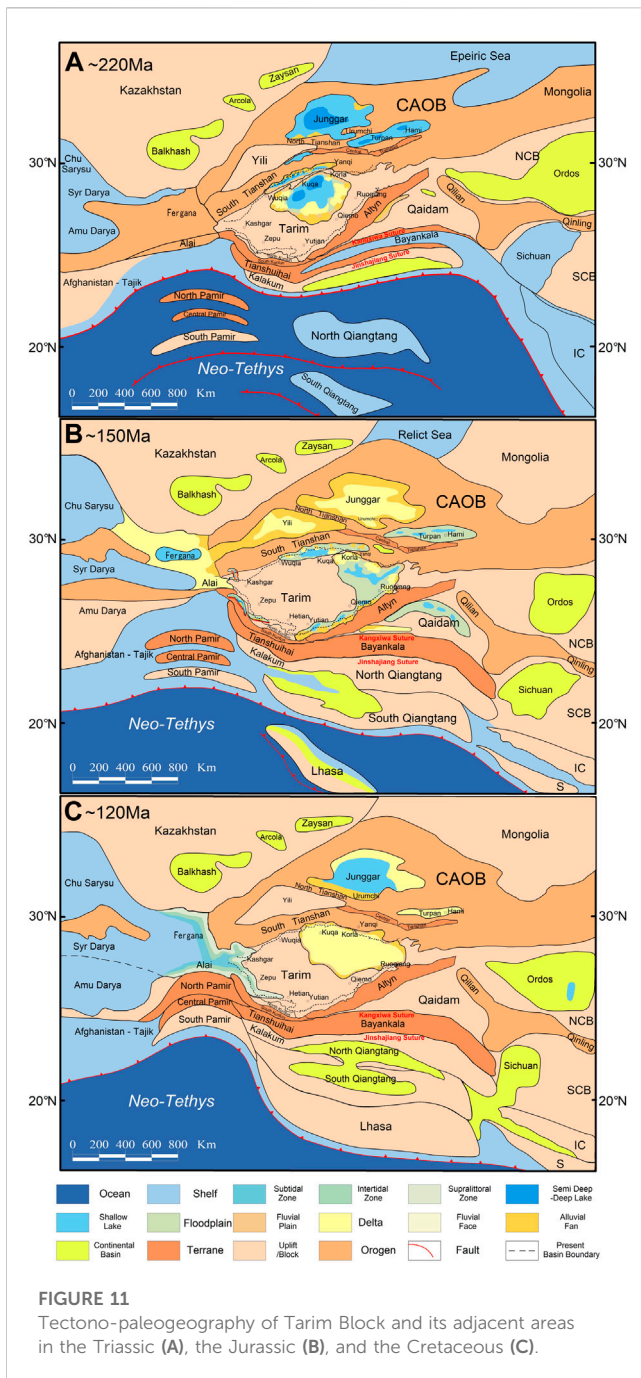
FIGURE 11
Tectono-paleogeography of Tarim Block and its adjacent areas in the Triassic **(A)**, the Jurassic **(B)**, and the Cretaceous **(C)**.

deposition, and the Kuqa Basin and the Central Basin have combined into a whole with red coarse clastic deposits (Figure 11C). The collision of the Lhasa Block with the Tarim Block formed an enormous compressional stress during the Late Early Cretaceous that caused the entire Tarim Basin to uplift and no longer accept sedimentation. The widespread transgression of the Tethys Ocean resulted in seawater influx from the western openings of the Tarim Basin into the southwestern Tarim Basin.

It began to receive a deposition of multiple mudstone-carbonate assemblages (~110 Ma).

6 Conclusion

1 The North Qiangtang Terrane and the South Qiangtang Terrane collided with the Tarim Block successively during ~220 Ma to 215 Ma, rather than merging into a single block before colliding in the late Triassic. This collision led to a large uplift in the southern Tarim Basin resulting in denudation of strata. Therefore, a large number of alluvial fans appeared in the southern margin of the sedimentary basin and the depositional center moved northward.

2 Faulted basins combined to form a large floodplain developed in the Early–Middle Jurassic extensional setting in the margins of the Tarim Basin. In the Late Jurassic, the Tarim Block was compressed to some extent and the faulted basin started to transform into a downwarped basin with red coarse clastic sediments as a result of the Amdo-Dongkacuo microcontinent collision with Tarim Block at ~160 Ma.

3 During the early Cretaceous period, the Tarim Basin was characterized by a downwarped basin inherited from the late Jurassic period. Around 120 Ma ago, the Lhasa Block collided with the Tarim Block, causing the Tarim Basin to experience uplift and denudation. Additionally, the southwestern region of the Tarim Basin underwent transgression from the Neo-Tethys Ocean, leading to the deposition of marine sediments.

Author contributions

XL did the main analysis, writing and editing. HC participated in the analysis and mapping of this paper. SH, CL, and YD provided extensive geological data and guidance. HZ, ZZ, JX, and LW have provided information from other eras as well as image making.

Conflict of interest

Authors SH, CL, and YD were employed by the company Tarim Oilfield Company.

The remaining authors declare that the research was conducted in the absence of any commercial or financial relationships that could be construed as a potential conflict of interest.

Publisher's note

All claims expressed in this article are solely those of the authors and do not necessarily represent those of their affiliated organizations, or those of the publisher, the editors and the reviewers. Any product that may be evaluated in this article, or claim that may be made by its manufacturer, is not guaranteed or endorsed by the publisher.

References

Bosboom, R., Dupont-Nivet, G., Grothe, A., Brinkhuis, H., Villa, G., Mandic, O., et al. (2014). Linking Tarim Basin sea retreat (west China) and Asian aridification in the late Eocene. *Basin Res.* 26 (5), 621–640. doi:10.1111/bre.12054

Chen, H. L., Luo, J. C., Guo, Q. Y., Liao, L., Cheng, X. G., Yang, S. F., et al. (2009). Deformation history and tectonic evolution of southeastern Tarim Basin in mesozoic and cenozoic. *Geotect. Metallogenia* 33 (1), 38–45.

Chen, R. L. (1995). Once more discussion on the middle jurassic marine-flooding event deposition of the Tarim Basin. *Exp. Pet. Geol.* 17 (4), 311–315.

Chen, R., Shen, Y. P., and Zhang, C. C. (2015). The Meso-Cenozoic tectono-palaeogeographic characteristics and evolution of Caribbean Plate margins. *J. Paleogeogr.* 17 (1), 63–81. doi:10.7605/gdlxb.2015.01.006

Chen, S. J., Zhao, Z. M., Ji, W. H., Li, R. S., Liu, R. L., and Zha, X. F. (2013). The characteristic of tectonic-lithofacies paleogeography during Early-Middle Permian in the west Kunlun and adjacent areas. *Chin. J. Geol.* 48 (4), 1015–1032. doi:10.3969/j.issn.0563-5020.2013.04.005

Chen, W. W., Yang, T. S., Zhang, S. H., Yang, Z. Y., Li, H. Y., Wu, H. C., et al. (2012). Paleomagnetic results from the early cretaceous zenong Group volcanic rocks, cuoqin, tibet, and their paleogeographic implications. *Gondwana Res.* 22 (2), 461–469. doi:10.1016/j.gr.2011.07.019

Chen, Y., Cogne, J. P., and Courtillot, V. (1992). New cretaceous paleomagnetic Poles from the Tarim Basin, northwestern China. *Earth Planet. Sci. Lett.* 114 (1), 17–38. doi:10.1016/0012-821x(92)90149-P

Eizenhöfer, P. R., and Zhao, G. (2018). Solonker suture in East Asia and its bearing on the final closure of the eastern segment of the palaeo-asian ocean. *Earth-Science Rev.* 186, 153–172. doi:10.1016/j.earscirev.2017.09.010

Fang, D. J., Chen, H. L., Wang, P. Y., and Tan, X. D. (1997). Paleomagnetic study and its tectonic significance for Tarim basin in Mesozoic. *Acta Geophys. Sin.* 40, 47–55.

Fang, D., Jin, G., Chen, H., Guo, Y., Wang, Z., Yin, S., et al. (1991). Preliminary approach to Late Paleozoic-Mesozoic geomagnetism and tectonic evolution in north margin of Tarim plate. *Res. Petroleum Geol. North. Tarim Basin China* 2, 96–104.

Fang, D. J., Shen, Z. Y., Ying, S. H., and Tan, X. D. (2001). Early cretaceous paleomagnetic results from the kuche depression, Tarim block and the cause of their inclination shallowing. *Chin. J. Geophys.* 44 (1), 68–78. doi:10.1002/cjg2.117

Feng, Z. Z., Peng, Y. M., Jin, Z. K., and Bao, Z. D. (2004). Lithofacies palaeogeography of the late ordovician in China. *J. Paleogeogr.* 6 (2), 128–139.

Fu, X. G., Wang, J., Tan, F. W., Chen, M., and Chen, W. B. (2010). The Late Triassic rift-related volcanic rocks from eastern Qiangtang, northern Tibet (China): Age and tectonic implications. *Gondwana Res.* 17 (1), 135–144. doi:10.1016/j.gr.2009.04.010

Gao, H. H., He, D. F., Tong, X. Y., Wen, Z. X., and Wang, Z. M. (2017). "Tectonic-depositional environment and proto-type basins evolution of the late ordovician in the Tarim Basin," in *Egu general assembly conference abstracts* (Vienna, Austria: EGUGA), 11218.

Gilder, S. A., Gomez, J., Chen, Y., and Cogne, J. P. (2008). A new paleogeographic configuration of the eurasian landmass resolves a paleomagnetic paradox of the Tarim Basin (China): A paleomagnetic paradox. *Tectonics* 27 (1), 2155. doi:10.1029/2007tc002155

Gilder, S., Chen, Y., Cogné, J. P., Tan, X., Courtillot, V., Sun, D., et al. (2003). Paleomagnetism of Upper Jurassic to Lower Cretaceous volcanic and sedimentary rocks from the Western Tarim Basin and implications for inclination shallowing and absolute dating of the M-0 (ISEA?) chron. *Earth Planet. Sci. Lett.* 206 (3-4), 587–600. doi:10.1016/s0012-821x(02)01074-0

Han, Y. G., and Zhao, G. C. (2018). Final amalgamation of the tianshan and junggar orogenic collage in the southwestern central asian orogenic belt: Constraints on the closure of the paleo-Asian ocean. *Earth-Science Rev.* 186, 129–152. doi:10.1016/j.earscirev.2017.09.012

He, B. Z., Jiao, C. L., Xu, Z. Q., Liu, S. L., Cai, Z. H., Li, H. B., et al. (2013a). Unconformity structural architecture and tectonic paleo-geographic environment: A case of the middle caledonian on the northern margin of tibet plateau and Tarim Basin. *Acta Petrol. Sin.* 29 (6), 2184–2198.

He, B. Z., Jiao, C. L., Xu, Z. Q., Cai, Z. H., Zhang, J. X., Liu, S. L., et al. (2016a). The paleotectonic and paleogeography reconstructions of the Tarim Basin and its adjacent areas (NW China) during the late Early and Middle Paleozoic. *Gondwana Res.* 30, 191–206. doi:10.1016/j.gr.2015.09.011

He, B. Z., Jiao, C. L., and Xu, Z. Q. (2015). Distribution and migration of the phanerozoic palaeo-uplifts in the Tarim Basin,NW. China. *Earth Sci. Front.* 22 (3), 277–289. doi:10.13745/j.esf.2015.03.024

He, D. F., Zhou, X., Zhang, C. J., and Yang, X. F. (2007). Tectonic types and evolution of Ordovician proto-type basins in the Tarim region. *Chin. Sci. Bull.* 52 (1), 164–177. doi:10.1007/s11434-007-6010-z

He, D. F., Jia, C. Z., Zhou, X. Y., Shi, X., Wang, Z. M., Pi, X. J., et al. (2005). Control principles of structures and tectonics over hydrocarbon accumulation and distribution in multi-stage superimposed basins. *ACTA PET. SIN.* 26 (3), 1–9.

He, D. F., Li, D. S., He, J. Y., and Wu, X. Z. (2013b). Comparison in petroleum geology between Kuga depression and Southwest depression in Tarim Basin and its exploration significance. *Acta Pet. Sin.* 34 (2), 201–218. doi:10.7623/syxb201302001

He, J., Wang, Y., Liu, S. L., and He, D. F. (2016b). Characteristics of fault structure and its control on hydrocarbon accumulation in the eastern part of southwestern Tarim Basin. *Petroleum Geol. Exp.* 38 (3), 326–332. doi:10.11781/sysydz20160332

Henry, P., and Natalya, A. (1996). Analysis of sonic well logs applied to erosion estimates in the Bighorn basin, Wyomin. *AAPG Bull.* 80 (5), 630–646.

Hou, G. T., Santosh, M., Qian, X. L., ister, G. S., and Li, J. H. (2008). Configuration of the Late Paleoproterozoic supercontinent Columbia: Insights from radiating mafic dyke swarms. *Gondwana Res.* 14 (3), 395–409. doi:10.1016/j.gr.2008.01.010

Hu, X. M., Ma, A. L., Xue, W. W., Garzanti, E., Cao, Y., Li, S. M., et al. (2022). Exploring a lost Ocean in the Tibetan plateau: Birth, growth, and demise of the bangong-nujiang ocean. *Earth-Science Rev.* 229, 104031. doi:10.1016/j.earscirev.2022.104031

Huang, B. C., Yan, Y. G., Piper, J. D. A., Zhang, D. H., Yi, Z. Y., Yu, S., et al. (2018). Paleomagnetic constraints on the paleogeography of the East Asian blocks during late paleozoic and early mesozoic times. *Earth-Science Rev.* 186, 8–36. doi:10.1016/j.earscirev.2018.02.004

Jia, C., and Wei, G. (1997). *Tectonic characteristics and petroleum, Tarim basin*. Beijing: China. Petrol. Ind. Press.

Jia, C. Z., Chen, H. L., Yang, S. F., Lu, H. F., and Zhou, Y. Z. (2003). Late Cretaceous uplifting process and its geological response in Kuqa Depression. *ACTA Pet. Sin.* 24 (3), 1–5.

Jia, C., Zhang, S., and Wu, S. (2004). *Stratigraphy of the Tarim Basin and adjacent areas*. (Beijing: Spinger, 1–450.

Jia, C. Z., Li, B. L., Lei, Y. L., and Chen, Z. X. (2013). The structure of Circum-Tibetan Plateau Basin-Range System and the large gas provinces. *Sci. China Earth Sci.* 43 (10), 1853–1863. doi:10.1007/s11430-013-4649-7

Jia, J. H. (2009). Sedimentary characteristics and paleogeography of the early cretaceous in Tarim Basin. *J. Paleogeogr.* 11 (2), 167–176.

Jin, Z. J., and Wang, Q. C. (2004). Recent developments in study of the typical superimposed basins and petroleum accumulation in China: Exemplified by the Tarim Basin. *Sci. China Ser. D-Earth Sci.* 47, 1–15. doi:10.1360/04zd0020

Jin, Z. J., Yang, M., Lu, X. X., Sun, D. S., Tang, X., Peng, G. X., et al. (2008). The tectonics and petroleum system of the Qiulitagh fold and thrust belt, northern Tarim Basin, NW China. *Mar. Petroleum Geol.* 25 (8), 767–777. doi:10.1016/j.marpetgeo.2008.01.011

Jolivet, M., Brunel, M., Seward, D., Xu, Z., Yang, J., Roger, F., et al. (2001). Mesozoic and cenozoic tectonics of the northern edge of the Tibetan plateau: Fission-track constraints. *Tectonophysics* 343 (1-2), 111–134. doi:10.1016/S0040-1951(01)00196-2

Laborde, A., Barrier, L., Simoes, M., Li, H., Coudroy, T., Van der Woerd, J., et al. (2019). Cenozoic deformation of the Tarim Basin and surrounding ranges (xinjiang, China): A regional overview. *Earth-Science Rev.* 197, 102891. doi:10.1016/j.earscirev.2019.102891

Lei, T., Zhang, H. Q., Jun, L., Zhang, N. C., and Shi, X. Q. (2020). Distribution of Nanhua-Sinian rifts and proto-type basin evolution in southwestern Tarim Basin, NW China. *Petroleum Explor. Dev.* 47 (6), 1206–1217. doi:10.1016/S1876-3804(20)60130-1

Li, C., Zhai, Q. G., Dong, Y. S., and Huang, X. P. (2006). Discovery of eclogite in central Qiangtang, qinghai-tibet plateau and its significance. *Chin. Sci. Bull.* 51 (1), 70–74.

Li, D., Liang, D., Jia, C., Wang, G., Wu, Q., and He, D. (1996). Hydrocarbon accumulations in the Tarim basin, China. *Aapg Bull.* 80 (10), 1587–1603.

Li, J. C., Zhao, Z. B., Zheng, Y. L., Yuan, G. L., Liang, X., Wang, G. H., et al. (2015). The magmatite evidences in southern Qiangtang for paleo-Tethys ocean subducting collision: Gangtang-co granites in Rongma, Tibet. *Acta Petrol. Sin.* 31 (7), 2078–2088.

Li, S., Yin, C. Q., Guilmette, C., Ding, L., and Zhang, J. (2019). Birth and demise of the bangong-nujiang tethyan ocean: A review from the gerze area of central tibet. *Earth-Science Rev.* 198, 102907. doi:10.1016/j.earscirev.2019.102907

Li, Y. A., Li, Q., Zhang, H., Sun, D. J., Cao, Y. D., and Wu, S. Z. (1995). Palaeomagnetic study of tarim and its adjacent area as well as the formation and evolution of Tarim Basin. *Xinjiang Geol.* 13 (4), 293–316.

Li, Y. (1990). An apparent polar wander path from the Tarim Block, China. *Tectonophysics* 181 (1-4), 31–41. doi:10.1016/0040-1951(90)90007-u

Li, Y., Qi, J. F., Shi, J., Sun, T., Xu, Z. P., Yu, H. B., et al. (2017). Microwave-assisted synthesis of imidazo[4,5-f] [1,10]phenanthroline derivatives as apoptosis inducers in chemotherapy by stabilizing bcl-2 G-quadruplex DNA. *Geotect. Metallogenia* 41 (5), 829–842. doi:10.3390/molecules22050829

Li, Y., Wen, L., Yang, X., Li, C., Zhang, L., Wang, B., et al. (2022). Mesozoic collision-related structures in the southern Tarim Basin, W. China: Implications for the paleo-tethys closing process. *Front. Earth Sci.* 9, 792049. doi:10.3389/feart.2021.792049

Li, Y., Zhang, Z., McWilliams, M., Sharps, R., Zhai, Y., Li, Y., et al. (1988). Mesozoic paleomagnetic results of the Tarim craton: Tertiary relative motion between China and Siberia? *Geophys. Res. Lett.* 15 (3), 217–220. doi:10.1029/gl015i003p00217

Li, Z. Y., Ding, L., Lippert, P. C., Song, P. P., Yue, Y. H., and van Hinsbergen, D. J. J. (2016). Paleomagnetic constraints on the mesozoic drift of the Lhasa terrane (tibet) from Gondwana to Eurasia. *Geology* 44 (9), 727–730. doi:10.1130/G38030.1

Lin, C., Li, S., Liu, J., Qian, Y., Luo, H., Chen, J., et al. (2011). Tectonic framework and paleogeographic evolution of the Tarim basin during the Paleozoic major evolutionary stages. *Acta Petrol. Sin.* 27 (1), 210–218.

Lin, C. S., Yang, H. J., Liu, J. Y., Rui, Z. F., Cai, Z. Z., and Zhu, Y. F. (2012). Distribution and erosion of the Paleozoic tectonic unconformities in the Tarim Basin, Northwest China: Significance for the evolution of paleo-uplifts and tectonic geography during deformation. *J. Asian Earth Sci.* 46, 1–19. doi:10.1016/j.jseaes.2011.10.004

Liu, J., Lin, C., and Jiang, L. (2000a). A quantitative model of compaction trend using sonic well logs: Applied to erosion amount estimation in the xihu depression, east China sea. *Petroleum Sci.* 4, 41–48.

Liu, J., Yi, J., and Chen, J. Y. (2020). Constraining assembly time of some blocks on eastern margin of Pangea using Permo-Triassic non-marine tetrapod records. *Earth-Science Rev.* 207, 103215. doi:10.1016/j.earscirev.2020.103215

Liu, L., Zhang, J. F., Cao, Y. T., Green, H. W., Yang, W. Q., Xu, H. J., et al. (2018). Evidence of former stishovite in UHP eclogite from the South Altyn tagh, Western China. *Earth Planet. Sci. Lett.* 484, 353–362. doi:10.1016/j.epsl.2017.12.023

Liu, Q., Zhao, G. C., Han, Y. G., Eizenhofer, P. R., Zhu, Y. L., Hou, W. Z., et al. (2017). Timing of the final closure of the paleo-Asian Ocean in the alxa terrane: Constraints from geochronology and geochemistry of late carboniferous to permian gabbros and diorites. *Lithos* 274, 19–30. doi:10.1016/j.lithos.2016.12.029

Liu, Q., Zhao, G. C., Sun, M., Eizenhofer, P. R., Han, Y. G., Hou, W. Z., et al. (2015). Ages and tectonic implications of neoproterozoic ortho- and paragneisses in the beishan orogenic belt, China. *Precambrian Res.* 266, 551–578. doi:10.1016/j.precamres.2015.05.022

Liu, Q., Zhao, G. C., Sun, M., Han, Y. G., Eizenhofer, P. R., Hou, W. Z., et al. (2016). Early paleozoic subduction processes of the paleo-Asian ocean: Insights from geochronology and geochemistry of paleozoic plutons in the alxa terrane. *Lithos* 262, 546–560. doi:10.1016/j.lithos.2016.07.041

Liu, Y. L., Hu, X. F., Wang, D. X., Zhao, Y., Zhang, Q., and Wen, L. (2012). Characteristics of triassic lithofacies palaeogeography in Tarim Basin. *Fault-Block Oil Gas Field* 19 (6), 696–700. doi:10.6056/dkyqt201206004

Liu, Z. H., Lu, H. F., Li, X. J., Jia, C. Z., Lei, G. L., Chen, C. M., et al. (2000b). Tectonic evolution of kuoa rejuvenated foreland basin. *Sci. Geol. Sin.* 35 (4), 482–492.

Ma, A. L., Hu, X. M., Kapp, P., BouDagher-Fadel, M., and Lai, W. (2020). Pre-oxfordian (>163 Ma) ophiolite obduction in central tibet. *Geophys. Res. Lett.* 47 (10), e2019GL086650. doi:10.1029/2019gl086650

Magara, K. (1976). Thickness of removed sedimentary-rocks, paleopore pressure, and paleotemperature, southwestern part of western Canada basin. *Aapg Bulletin-American Assoc. Petroleum Geol.* 60 (4), 554–565.

Mattern, F., and Schneider, W. (2000). Suturing of the proto- and paleo-tethys oceans in the Western Kunlun (xinjiang, China). *J. Asian Earth Sci.* 18 (6), 637–650. doi:10.1016/S1367-9120(00)00011-0

Mcfadden, P. L., Ma, X. H., Mcelhinny, M. W., and Zhang, Z. K. (1988). Permo-triassic magnetostratigraphy in China - northern Tarim. *Earth Planet. Sci. Lett.* 87 (1-2), 152–160. doi:10.1016/0012-821x(88)90071-4

Meng, Z., Deng, Y., Ding, Z., Zheng, Y., Li, Y. a., and Sun, D. (1998). New paleomagnetic results from Ceno-Mesozoic volcanic rocks along southern rim of the Tarim Basin, China. *Sci. China Ser. D Earth Sci.* 41 (2), 91–104. doi:10.1007/bf02984517

Qi, J., Li, Y., Xu, Z., Yang, S., and Sun, T. (2022). A structural interpretation model and restoration of the mesozoic proto-basin for the Kuqa depression, Tarim Basin. *Acta Geol. Sin. Ed.* 97, 207–225. doi:10.1111/1755-6724.14963

Qu, G. S., Zhang, N., Liu, J., Li, Y. G., and Li, Y. F. (2004). Structural deformation mechanism of Meso-Cenozoic basement and cover in the north Tarim uplift-Kuqa depression. *Geol. Bull. China* 23 (2), 113–119.

Shen, Z., Chen, H., Fang, D., Ding, J., Zhang, S., Huang, Z., et al. (2005). Paleomagnetic results of the Cretaceous marine sediments in Tongyouluke, southwest Tarim. *Sci. China Ser. D Earth Sci.* 48 (3), 406–416. doi:10.1360/03yd0378

Sobel, E. R. (1999). Basin analysis of the jurassic–lower cretaceous southwest Tarim basin, northwest China. *Geol. Soc. Am. Bull.* 111 (5), 709–724. doi:10.1130/0016-7606(1999)111<0709:baotjl>2.3.co;2

Song, C., Wang, J., Fu, X., Feng, X., Chen, M., and He, L. (2012). Late Triassic paleomagnetic data from the Qiangtang terrane of Tibetan Plateau and their tectonic significances. *J. Jilin Univ.* 42 (2), 526–535.

Song, P. P., Ding, L., Li, Z. Y., Lippert, P. C., Yang, T. S., Zhao, X. X., et al. (2015). Late triassic paleolatitude of the Qiangtang block: Implications for the closure of the Paleo-Tethys Ocean. *Earth Planet. Sci. Lett.* 424, 69–83. doi:10.1016/j.epsl.2015.05.020

Van der Voo, R. (1990). Phanerozoic paleomagnetic poles from Europe and North America and comparisons with continental reconstructions. *Rev. Geophys.* 28 (2), 167–206. doi:10.1029/RG028i002p00167

Wang, C. S., Zheng, H. R., Ran, B., Liu, B. P., Li, X. H., Li, Y. L., et al. (2010). On paleogeographic reonstruction: An example for application in Tibetan Tethys. *Acta Sedimentol. Sin.* 28 (5), 849–860.

Wang, Q., Li, S. Z., Zhao, S. J., Mu, D. L., Guo, R. H., and Somerville, Ian. (2017). Early paleozoic Tarim orocline: Insights from paleogeography and tectonic evolution in the Tarim Basin. *Geol. J.* 53 (12), 436–448. doi:10.1002/gj.2985

Wang, T., Jin, Z., Shi, Z., Dai, X., and Cheng, R. (2020). Phanerozoic plate history and structural evolution of the Tarim Basin, northwestern China. *Int. Geol. Rev.* 62 (12), 1555–1569. doi:10.1080/00206814.2019.1661038

Wang, Y. C. (2004). Paleomagnetic result of the cretaceous-cenozoic basalts from the Tuoyun Basin, southwestern tianshan of China and its tectonic implications. *Chin. Sci. Bull.* 49. 1288–1295.

Wang, Y. S., Qu, Y. G., Sun, Z. G., Zheng, C. Z., Xie, H. Y., and Lu, Z. L. (2007). Characteristics and tectonic setting of volcanic rocks of the Late Triassic Nongbai Formation at the northern margin of south Qiangtang block, northern Tibet, China. *Geol. Bull. China* 26 (6), 682–691.

Wei, B. T., Cheng, X., Domeier, M., Jiang, N., Wu, Y. Y., Zhang, W. J., et al. (2022). Placing another piece of the tethyan puzzle: The first paleozoic paleomagnetic data from the South Qiangtang block and its paleogeographic implications. *Tectonics* 41 (10), e2022TC007355. doi:10.1029/2022tc007355

Wei, G. Q., Zhu, Y. J., Zheng, J. F., Yu, G., Ni, X. F., Yan, L., et al. (2021). Tectonic-lithofacies paleogeography, large-scale source-reservoir distribution and exploration zones of Cambrian subsalt formation, Tarim Basin, NW China. *Petroleum Explor. Dev.* 48 (6), 1289–1303. doi:10.1016/S1876-3804(21)60287-2

Wu, G. H., Deng, W., Huang, S. Y., Zheng, D. M., and Pan, W. Q. (2020). Tectonic-paleogeogr.phic evolution in the Tarim Basin. *Chin. J. Geol.* 55 (2), 305–321. doi:10.12107/dzkx.2020.020

Wu, G., Lin, C., Yang, H., Liu, J., Liu, Y., Li, H., et al. (2019). Major unconformities in the mesozoic sedimentary sequences in the kuqa–tabei region, Tarim Basin, NW China. *J. Asian Earth Sci.* 183, 103957. doi:10.1016/j.jseaes.2019.103957

Wu, H. X., Cheng, X. G., Chen, H. L., Chen, C., Dilek, Y., Shi, J., et al. (2021). Tectonic switch from triassic contraction to jurassic-cretaceous extension in the western Tarim Basin, northwest China: New insights into the evolution of the paleo-tethyan orogenic belt. *Front. Earth Sci.* 9, 636383. doi:10.3389/feart.2021.636383

Xi, D., Tang, Z., Wang, X., Qin, Z., Cao, W., Jiang, T., et al. (2020). The Cretaceous-Paleogene marine stratigraphic framework that records significant geological events in the Western Tarim Basin. *Earth Sci. Front.* 27 (6), 165.

Xia, J. K., Zhong, Z. Q., Huang, S. Y., Luo, C. M., Lou, H., Chang, H. N., et al. (2023). The proto-type basin and tectono-paleogeographic evolution of the Tarim basin in the Late Paleozoic. *Front. Earth Sci.* 11, 1097101. doi:10.3389/feart.2023.1097101

Xiao, W. J., Han, F. L., Windley, B. F., Yuan, C., Zhou, H., and Li, J. L. (2003). Multiple accretionary orogenesis and episodic growth of continents: Insights from the Western Kunlun Range, central Asia. *Int. Geol. Rev.* 45 (4), 303–328. doi:10.2747/0020-6814.45.4.303

Xiao, W. J., Windley, B. F., Hao, J., and Li, J. L. (2002). Arc-ophiolite obduction in the western Kunlun range (China): Implications for the palaeozoic evolution of central Asia. *J. Geol. Soc.* 159 (5), 517–528. doi:10.1144/0016-764901-093

Xiao, W. J., Windley, B. F., Sun, S., Li, J. L., Huang, B. C., Han, C. M., et al. (2015). A tale of amalgamation of three permo-triassic collage systems in central Asia: Oroclines, sutures, and terminal accretion. *Annu. Rev. Earth Planet. Sci.* 43 (43), 477–507. doi:10.1146/annurev-earth-060614-105254

Xu, Z. Q., Li, S. T., Zhang, J. X., Yang, J. S., He, B. Z., Li, H. B., et al. (2011). Paleo-asian and tethyan tectonic systems with docking the Tarim block[J]. *Acta Petrol. Sin.* 27 (1), 1–22.

Yang, K. (1994). The formation and evolution of the Western Kunlun continental margin. *Geol. Rev.* 40 (1), 9–18.

Yang, P. X., Tian, J. C., and Zhang, X. (2019). Study of characteristics of Triassic sedimentary facies and depositional model in the northern Shunbei region, Tarim basin. *Mineralogy Petrology* 39 (4), 86–96. doi:10.19719/j.cnki.1001-6872.2019.04.10

Yu, H. B., Qi, J. F., Yang, X. Z., Liu, Q. Y., Cao, S. J., Fan, S., et al. (2016). The mesozoic tectonic palaeogeographic analysis in Kuqa depression of Tarim Basin. *Geol. J. China Univ.* 22 (4), 657–669. doi:10.16108/j.issn1006-7494.2016021

Zhang, C. S., Xiao, A. C., Li, J. Y., and Shi, D. (2000). Depositional feature of jurassic fault BASIN IN southwest Tarim depression. *J. Mineral Pet.* 20 (3), 41–45. doi:10.19719/j.cnki.1001-6872.2000.03.008

Zhang, S. J., Hu, X. M., Han, Z., Li, J., and Garzanti, E. (2018). Climatic and tectonic controls on Cretaceous-Palaeogene sea-level changes recorded in the Tarim epicontinental sea. *Palaeogeogr. Palaeoclimatol. Palaeoecol.* 501, 92–110. doi:10.1016/j.palaeo.2018.04.008

Zhang, X. Z., Dong, Y. S., Li, C., Xie, C. M., Wang, M., Deng, M. R., et al. (2014). A record of complex histories from oceaniclithosphere subduction to continental subduction and collision: Constraints on geochemistry of eclogite and blueschist in Central Qiangtang,Tibetan Plateau. *Acta Petrol. Sin.* 30 (10), 2821–2834.

Zhang, Z. K., Li, Y. A., and Li, Q. (1989). Jurassic and cretacious paleomagnetism of the Tarim block. *Seismol. Geol.* 11 (3), 9–16.

Zhao, G. C., Wang, Y. J., Huang, B. C., Dong, Y. P., Li, S. Z., Zhang, G. W., et al. (2018). Geological reconstructions of the East Asian blocks: From the breakup of rodinia to the assembly of pangea. *Earth-Science Rev.* 186, 262–286. doi:10.1016/j.earscirev.2018.10.003

Zheng, M. L., Wang, Y., Jin, Z. J., Li, J. C., Zhang, Z. P., Jiang, H. S., et al. (2014). Superimposition, evolution and petroleum accumulation of Tarim Basin. *Oil Gas Geol.* 35 (6), 925–934. doi:10.11743/ogg20140619

Zhong, Z. Q., Xia, J. K., Huang, S. Y., Luo, C. M., Chang, H. N., Li, X., et al. (2023). Reconstruction of proto-type basin and tectono-paleogeography of Tarim Block in early Paleozoic. *Front. Earth Sci.* 11, 1101360. doi:10.3389/feart.2023.1101360

Zhou, Z., Zhao, Z., and Hu, Z. (2001). *Stratigraphy of the Tarim Basin*. Beijing: Sci. Press, 1–359.